Piezoelectric polar nanoregions and relaxation-coupled resonances in relaxor ferroelectrics

Ling Cai, Radha Pattnaik, Joel Lundeen, and Jean Toulouse*
Physics Department, Lehigh University, Bethlehem, Pennsylvania 18015, USA

(Received 14 July 2017; revised manuscript received 2 October 2018; published 25 October 2018)

It is a generally accepted fact that the unique dielectric properties of relaxor ferroelectrics are related to the formation of polar nanoregion (PNRs). Less well recognized is the corollary that, because they are polar and therefore lack inversion symmetry, PNRs are also piezoelectric at the nanoscale and can therefore behave as nanoresonators. Using the particular relaxor ferroelectric $K_{1-x}Li_xTaO_3$ (KLT), we show that, when electrically excited into oscillation, these piezoelectric nanoresonators can drive macroscopic electromechanical resonances. Unexpectedly, however, pairs of coupled resonances corresponding to a particular type of oscillation are observed, with one of the resonance exhibiting a characteristic Fano-like line shape. The complex resonance spectra can be described equally well by two alternative but complementary models both involving two resonances coupled through a relaxation: a purely classical one based on two coupled damped harmonic oscillators and a semiclassical based on two discrete excitations coupled to each other through a continuum. Together, they provide complementary perspectives on the underlying physics of the system. Both reproduce the rapid evolution of the resonance spectrum across three wide temperature ranges, including a phase transition range. In the high-temperature range, the coupling between modes is due to the collective π relaxation of the lithium ions within PNRs and, in the phase transition range, to "heterophase relaxation" of the surrounding lattice between its high-temperature cubic and low-temperature tetragonal phases, both coherent effects. The coupling is suppressed in the intermediate range of the collective $\pi/2$ relaxation of the lithium ions. Incidentally, the measured dielectric spectra are shown to bear a surprising but justifiable resemblance to the optical spectra of certain atomic vapors exhibiting electromagnetically induced transparency.

DOI: 10.1103/PhysRevB.98.134113

I. INTRODUCTION

$K_{1-x}Li_xTaO_3$ (KLT), $KTa_{1-x}Nb_xO_3$ (KTN), $PbMg_{1/3}Nb_{2/3}O_3$-$PbTiO_3$ (PMN-PT), $PbZn_{1/3}Nb_{2/3}O_3$-$PbTiO_3$ (PZN-PT), and $PbSc_{1/2}Nb_{1/2}O_3$ (PSN) belong to the family of relaxor ferroelectrics (RF). RFs are highly polarizable mixed compounds in which substituted cations are off-centered already in the paraelectric phase, forming a dipole that can reorient between several crystallographically equivalent directions. At lower temperatures, interactions between off-center ions in the highly polarizable lattice result in the formation of lower symmetry (i.e., permanent) polar nanoregions (PNR) [1,2], the size of which can be estimated from neutron and x-ray elastic diffuse scattering [3,4]. Although the term polar nanoregions or PNRs is widely used in the RF literature, it would be preferable in the present paper to label these polar nanodomains or PNDs [5] so as to emphasize the long-lived or permanent character of the local distortion and lower local symmetry of these regions below a certain temperature, T^*, both features that are essential in explaining the results reported here. Because of the general practice in the RF literature however, we keep here the PNR label. Due to their mixed composition and resulting complex structural features, RFs exhibit unique local as well as lattice dynamics, the most characteristic feature of which is the strong frequency dispersion of their dielectric constant commonly identified as "the relaxor behavior" [6,7]. This dispersion is due to the relaxation of the PNRs between different orientations. Simultaneously, when subjected to relatively small dc electric fields, relaxor ferroelectrics (RF), exhibit unusual electromechanical resonances (EM) [8] that are clearly associated with the presence of these PNRs coupling polarization and strain. Similar resonances have also been observed in nanocomposites [9] and are interesting for two reasons. First, they provide a sensitive tool to probe the interplay between local and lattice dynamics which is at the core of the behavior of these complex solids. Secondly, they form the basis for the primary applications of RFs in transducers and actuators [10,11]. In an earlier paper [12], we reported the first observation of new resonances in KTN and KLT and interpreted them as evidence for the formation of permanent polar nanodomains in the "paraelectric" relaxor phase. In a follow up paper [13], we developed a phenomenological Debye model involving electrostrictive polarization-strain coupling to describe this resonance. This two papers focused on the primary (broad) resonance as a signature of the PNRs and their electrostrictive properties, as we did not yet recognize at the time the importance of the secondary (narrow) resonance, the meaning of its characteristic spectral shape and its relationship to the primary resonance. In the present paper, we report the results of a comprehensive and detailed study of these resonances in the relaxor KLT over a wide range of temperatures and frequencies. Most importantly, we now identify pairs of *coupled resonances* (primary and secondary), uncover their origin and describe

*jt02@lehigh.edu

the coherent coupling mechanism that gives rise to their characteristic spectral shapes. These spectral shapes are seen to evolve rapidly with decreasing temperature, first due to their interaction with the relaxations mentioned above, and then to the occurrence of a phase transition. In the vicinity of the phase transition, they provide evidence for the existence of "heterophase fluctuations" of the system between its high-temperature cubic and low-temperature tetragonal phase [14].

In KLT, lithium ions are off-centered from the normal crystallographic site by almost 1 Å, thus forming electric dipoles that can reorient among six equivalent cubic directions [15,16]. At lower temperature, interactions between off-center lithium ions result in their displacements becoming correlated, leading to a local transition and the appearance of tetragonal polar nanoregions [4]. PNRs exhibit two distinct types of local dynamics. First, they can relax between several crystallographically equivalent orientations via collective 90° and 180° jumps of the Li dipoles [17,18]. Secondly, being polar and therefore lacking inversion symmetry, they are also piezoelectric and can exert a stress on the surrounding lattice to drive a crystal bar into electromechanical resonance. Similar resonances have also been observed in KTN and PZN. Given the common characteristics of relaxor ferroelectrics (off-center mixed ions and a high polarizability), the results reported below should be indicative of the behavior of other RFs as well, and to provide a more complete picture of the inter-relationship between mesoscopic and macroscopic dynamics in these compounds. With regards to applications, these results may also contribute to a better understanding of the piezoelectric properties of nanocomposites.

In the next Experimental and Results section, we present the dielectric constant and electromechanical results on the two crystals studied. In the Analysis section, we fit the resonance spectra with two different theoretical models, providing complementary perspectives on the underlying physics. Finally, in the Physical Model and Discussion section, we describe schematically the underlying physics of the two models and highlight their special meaning.

II. EXPERIMENTAL DETAILS AND RESULTS

Two KLT single crystals were grown from solution by the slow cooling method at Oak Ridge National Laboratory. The nominal lithium concentrations of these two crystals were $x = 3.5\%$ and 10%. However, using a formula proposed earlier to calculate concentrations of lithium based on the transition temperature [19], we estimate that actual concentrations in our crystals were respectively 2.6% and 4.7%, both therefore exceeding the critical concentration of $\leqslant 2\%$. The crystals were cut along (100) faces in the form of bars with approximate dimensions $5\times2\times1$ mm. Metallic electrodes were evaporated on the two largest parallel surfaces of the samples. In order to rule out possible electrode-sample interface effects, different coating/interface conditions, such as sputtered gold, vapor deposited aluminum and painted silver, were tested to ensure that the same dielectric results were obtained. Different grades of surface polish were also tested, from rough to optical grade, and the same dielectric results were obtained in all cases.

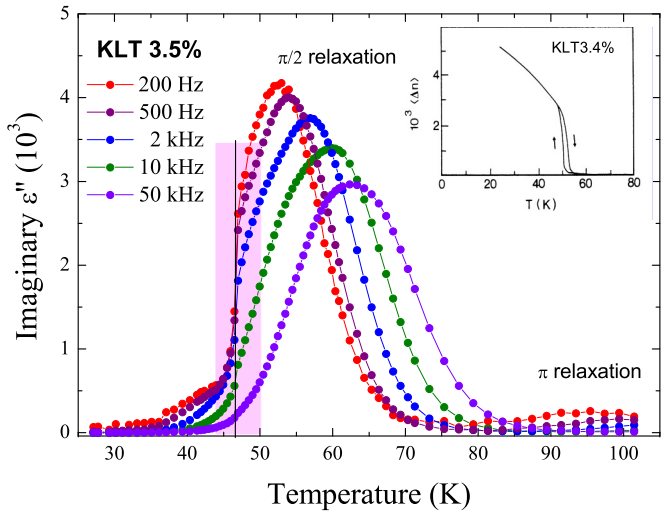

FIG. 1. Imaginary part of the dielectric constant of KLT3.5% measured at different frequencies. The hatched area marks the transition region III (see text below). (Inset) Birefringence of a different KLT3.4% crystal [21].

Ultimately, aluminum electrodes were used. The samples were held stress-free inside an open cycle cryostat. For the dielectric relaxation measurements, a small ac electric field (0.5 V/cm) was applied across the short dimension (thickness) of the crystal sample. The parallel plate capacitance and the loss tangent were measured with a HP4194A network analyzer, sweeping the frequency from 100 Hz to 10 MHz. The measured capacitance was converted to a dielectric constant through the relation $\epsilon' = Cd/A\epsilon_0$, where C is the capacitance, d the sample thickness, A the area of the electrode and ϵ_0 the free space permittivity. The samples were cooled with liquid helium from room temperature to ~20 K. The cooling rate was controlled to be on average 0.2 K/min but the temperature was equilibrated at each measuring temperature, allowing sufficient time for the sample to reach thermal equilibrium before each measurement, as monitored by the stability of the capacitance value at that temperature.

Figure 1 shows the imaginary part of the dielectric permittivity (absorption) of the $K_{1-x}Li_xTaO_3$ (KLT) crystal with an actual concentration of 2.6% Li (nominal 3.5%), measured upon cooling as a function of temperature and at several frequencies. Two relaxation peaks are visible. The small peak at ~95 K corresponds to the 180° reorientation or π relaxation and the large peak at lower temperature to the 90° reorientation or $\pi/2$ relaxation of the PNRs under the effect of the external ac field [16]. The weaker strength of the π relaxation in KLT3.5% is due to the fact that the corresponding distortion (or elastic quadrupole) is in principle the same for both crystallographic orientations (zero or π) of the PNRs but for the piezoelectric effect. The transition to the tetragonal phase is evidenced by several experimental observations, probably the most direct of which are the sharp drop in the dielectric constant at $T_c \approx 47$ K and a doubling of the phonon peaks detected in a neutron inelastic scattering study of KLT3.5% [20]. The inset in Fig. 1 also shows birefringence results obtained under continuous cooling and warming (no

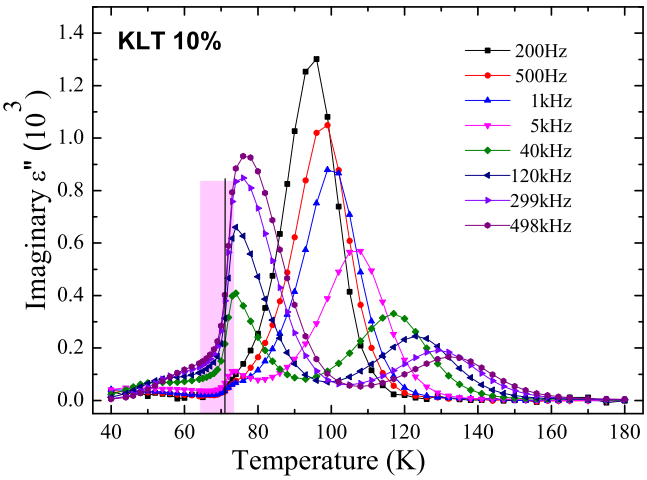

FIG. 2. Imaginary part of the dielectric constant of KLT10% measured at different frequencies. The high-temperature peak corresponds to the π relaxation and the low-temperature peak (interrupted by the transition), to the $\pi/2$ relaxation. The hatched area marks the transition region III (see text below).

equilibration) in a KLT crystal with nominal 3.4% lithium [21]. Instead of a single curve, these reveal a narrow thermal hysteresis loop (see also Ref. [22]), which signals the existence of a two-phase region around the transition. Fluctuations between these two phases can therefore be expected in the vicinity of the transition (see later discussion on heterophase fluctuations) [23]. In this regard, it is useful to note in Fig. 1 that the width of the thermal hysteresis in the KLT3.4% crystal is approximately the same as that of the hatched area on the dielectric curve of the KLT3.5% crystal, which represents the transition region ($T_c \pm 4$ K) to be examined below.

For comparison, the corresponding dielectric results obtained on the KLT crystal with an actual $x = 4.2\%$ Li concentration (nominal 10%) are presented in Fig. 2. For this higher concentration, the π relaxation peak is much more prominent than in KLT3.5, possibly due to the larger size of the polar nanoregions and stronger strain fields. At the lower frequencies, the $\pi/2$ relaxation peak is not fully developed, being cut off by the intervening transition. Stated otherwise, the structural transition in KLT10% intervenes at a higher temperature than that at which the $\pi/2$ relaxation peak would normally be observed if the transition did not occur.

Relaxor ferroelectrics (RFs) also exhibit characteristic resonances, precisely in the same temperature region in which the PNRs are present and undergoing the $\pi/2$ and π relaxations mentioned above (see also Ref. [12]). For the measurements of these dielectric resonances, the same configuration was used as for the dielectric relaxation measurements save for a modest dc electric field (~370 V/cm) that was applied to partially align the PNRs and induce a small but nonzero macroscopic polarization. The frequency of the small measuring ac electric field was then swept through the resonance, the frequency of which can be calculated from the dimension of the crystal bar L, the density $\rho = 7.02$ g/cm^3, and the elastic constant $C_{11} \approx 4\times10^{12}$ dynes/cm^2, as $\nu = \frac{1}{2L}\sqrt{\frac{C_{11}}{\rho}}$ [12]. The results are presented in Fig. 3 in the form of the dielectric loss tangent, $D \equiv \epsilon''/\epsilon'$.

The frequencies of both resonances are found to fall within the same range as for length mode (longitudinal) oscillations, associated with the longitudinal strain (ϵ_{11}) of the bar, i.e., perpendicular to the direction of the applied electric field (E_3), associated with the C_{11} elastic modulus and corresponding to the d_{311} piezoelectric coefficient. The long dimension of the crystal bar samples was sufficiently different from the two others so as to exclude the possibility that the two resonances observed might correspond to two distinct modes of vibration (width thickness). The resonance frequencies on the KLT3.5 sample measured here were also found to be very close to those measured in KTN samples with similar sample dimensions. It is important to note that, while the PNRs are piezoelectric (lack of local inversion symmetry), the rest of the crystal is not (being cubic and with inversion symmetry). Hence it is the PNRs that are excited into piezoelectric oscillations, thereafter driving the macroscopic oscillations of the bar. Unexpectedly, not one but a pair of resonances is observed starting approximately at 120 K, the temperature at which the (quasistatic or static) PNRs are known to appear as determined from independent measurements mentioned above (Raman [2] and diffuse neutron scattering [4]). The more intense of the two resonances is broad and symmetric and the less intense is narrow and presents a characteristic asymmetry. It is important to note that these resonances are only observed upon appearance of the PNRs and have been observed reproducibly in several crystals. They cannot therefore be due to sample size or electrode effects.

The evolution of the resonances can be divided in three stages: (i) region I, the π relaxation range, (ii) region II, the $\pi/2$ relaxation range, and (iii) region III, the transition range. In region I, both resonances appear and grow in amplitude, with the narrow resonance becoming equal in strength to the broad resonance. One major difference however is that the frequency of the narrow resonance remains constant with changing temperature, while that of the broad resonance continuously decreases in frequency, (anti)-crosses over the narrow one at the temperature in the temperature region of the π relaxation maximum. At their point of closest approach ($T \approx 96$ K in Fig. 3), both resonance peaks are almost equal in strength and width, suggesting an energy exchange between them. In region II, the narrow resonance progressively disappears while the frequency of the broad resonance continues to decrease with decreasing temperature, becoming strongly damped as it approaches the $\pi/2$ relaxation. It is important to note that, compared to the resonance peaks, the relaxation peak is much broader and shifts rapidly with temperature. Consequently, the relaxation peak appears only as a sloped background within the limited frequency range used to display the resonances and its slope changes sign between 70 and 58 K as it crosses over the $\pi/2$ relaxation. In region III, approaching the transition and with the $\pi/2$ relaxation now much too slow and therefore no longer active in dampening the resonances, both reappear and the broad resonance again increases in frequency and decreases in width. At 44 K, the two resonances are again close to each other in frequency, resulting this time in a spectrum that superficially looks like

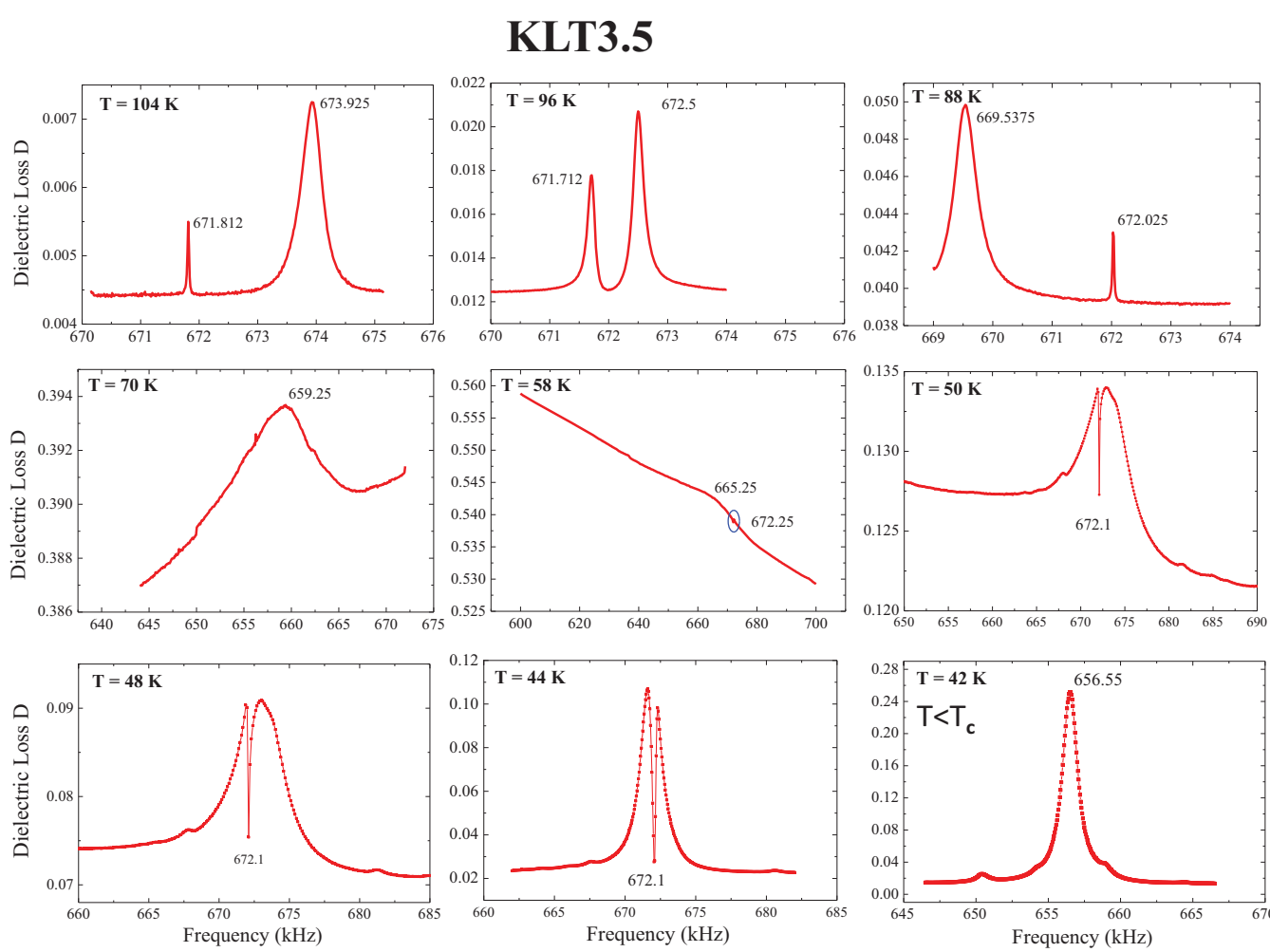

FIG. 3. Evolution with temperature of the dielectric loss, $D \equiv \epsilon''/\epsilon'$, of KLT3.5. As discussed in the text, the spectra shown can be grouped into four regions: 104–88 K in region I of the π relaxation, 70 K–58 K in region II of the $\pi/2$ relaxation, 50–44 K in region III of the transition, and 42 K below T_c. The broad resonance couples strongly to the narrow one as they are closest to each other just below 96 K. Below 70 K, the broad resonance peak rides over the $\pi/2$ relaxation peak and is strongly damped at 58 K. At 50 K, both the broad and narrow resonance peaks have reappeared. And below the phase transition region, only the broad resonance is active (see explanation in text).

a broad peak split in the middle. Throughout, the broad resonance shifts in frequency but the narrow resonance remains at approximately the same frequency. Finally, at 42 K and below for KLT3.5, only the broad resonance is observed. The corresponding real parts of the dielectric permittivity are also shown in Fig. 4 at two temperatures within the transition range and below. Strikingly, below the transition a single resonance is observed.

Very similar resonance spectra are observed in the KLT10 (4.7% Li) crystal and are presented in Fig. 5. The evolution of the resonances is very similar to that in the KLT3.5 (2.6% Li) crystal, with the same three temperature ranges: (i) the π relaxation range, (ii) the $\pi/2$ relaxation range, and (iii) the transition range. At this higher concentration, both the π relaxation and $\pi/2$ relaxation peaks are now clearly visible in Fig. 2 in addition to the resonances. However, for the reason mentioned in the previous paragraph, in Fig. 5 they are only seen as a sloped background in the narrow frequency intervals of the resonance spectra. As the π relaxation crosses the resonances, between 112 and 105 K, the slope of the background changes from negative to positive. As explained below, the fact that the broad resonance (anti)-crosses the narrow one, and itself becomes equally narrow in this temperature range which also coincides with the π relaxation

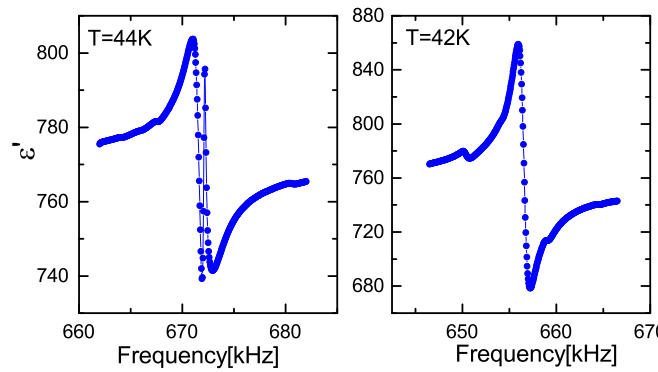

FIG. 4. Real part of the dielectric constant of KLT3.5 in the transition region (hatched area in Fig. 1) and just below.

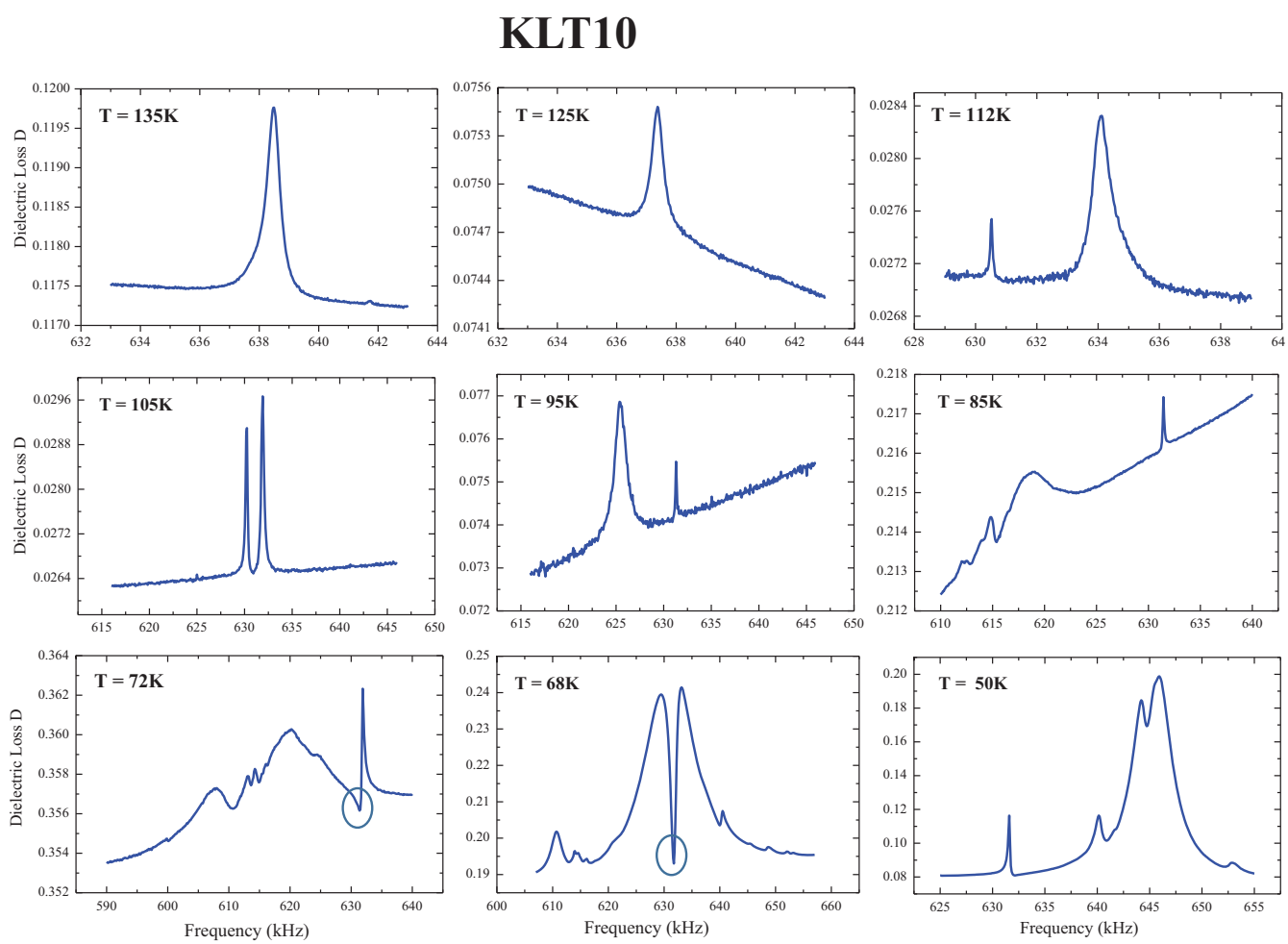

FIG. 5. Evolution with temperature of the dielectric loss, $D \equiv \epsilon''/\epsilon'$, of KLT10. As discussed in the text, the spectra shown can be grouped into four regions: 135–105 K in region I of the π relaxation, 85–72 K in region II of the $\pi/2$ relaxation, 68 K in region III of the transition, and 50 K below T_c. The broad resonance is seen to strongly couple to the narrow one as they are nearest to each other at 105 K. This temperature also corresponds approximately to the temperature at which the slope of the background goes from being negative to being positive vs frequency, i.e., where the π relaxation crosses the resonances, as seen from Fig. 2. Note the anticrossing of the two resonances at 105 K and the antiresonance between 72 and 55 K (latter not shown), indicating the coherent character of the interaction [27].

maximum, suggests that the two resonances are coupled via the relaxation. A sloped background is also observed in region II of the $\pi/2$ relaxation, but the slope is not seen changing sign because the relaxation peak is cut short by the intervening transition, now at higher temperature for this higher concentration crystal. The additional small peaks that are seen at the lower temperatures in the spectra of Figs. 3 and 5 are not understood at this time. They are much smaller in amplitude and do not affect the interpretation of the main features (broad and narrow peaks) reported here. Figure 6 presents the resonance spectra (real and imaginary) from KLT10. They are very similar in shape to those of KLT3.5, but broader in frequency, which reflects a lower Q factor at this higher concentration.

The frequency evolution of the broad and narrow resonances is summarized in Figs. 7 and 8 for the KLT3.5 and KLT10 crystals respectively, together with the temperature evolution of the real part of the dielectric constant measured without an external dc field at 50 kHz for KLT3.5 and at 40 and 498 kHz for KLT10. On the high-temperature side, the broad and narrow resonances (anti)-crosses in the region of the π relaxation. In the intermediate-temperature range, the frequency of the broad resonance decreases rapidly and reaches a minimum at approximately the same temperature as

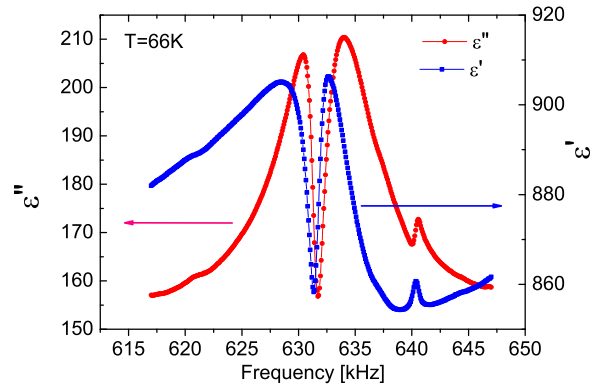

FIG. 6. Real and imaginary parts of the dielectric constant of KLT10 in the transition region (hatched area in Fig. 2).

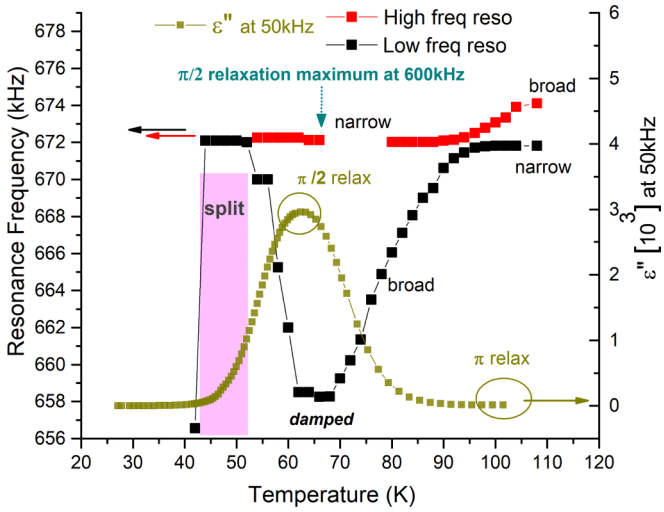

FIG. 7. Frequencies of the narrow and broad resonances in KLT3.5 as a function of temperature. Note the anticrossing of the broad and narrow resonance at $T \approx 95$ K, which is also the temperature region of the π relaxation maximum of the imaginary part of the dielectric constant measured at high frequency in Fig. 1. The $\pi/2$ relaxation maximum is also shown here to fall in the temperature range of the minimum frequency of the broad resonance.

that of the maximum of the $\pi/2$ relaxation (when measured at the same frequency as the resonance). It then increases rapidly upon approaching the phase transition, where the two resonances again meet. In the next Analysis section, we show that the resonance spectra presented above can be described equally well by two complementary models, each reflecting a different aspect of the resonance-relaxation dynamics. In the subsequent Discussion section, we then describe the physical mechanisms that explain the evolution with temperature of the dielectric resonance spectra.

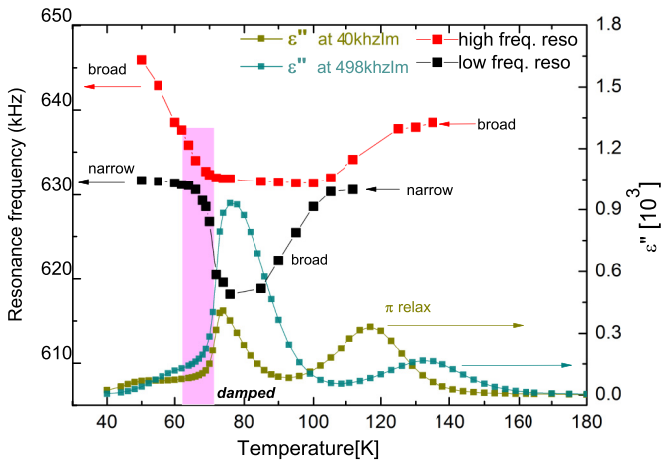

FIG. 8. Frequencies of the narrow and broad resonances in KLT10 as a function of temperature. Note the anticrossing of the broad and narrow resonance a $T \approx 110$ K, in the temperature region of the π relaxation maximum of the imaginary part of the dielectric constant in Fig. 2. The $\pi/2$ relaxation maximum is also shown here to fall in the temperature range of the minimum frequency of the broad resonance.

III. ANALYSIS

In the present section, we show that the observed spectra in all three separate temperature regions identified above can be accurately described by either one of two models, the first one purely classical and phenomenological and the second one semi-classical, providing complementary perspectives on the results. Both models are shown to describe equally well the spectral shapes in regions I and III in terms of two resonances coupled by a relaxation, the π relaxation in region I and the heterophase relaxation in region III (see below). In the intermediate region II, the $\pi/2$ relaxation dominates and dampens the resonances. In what follows, we first establish the physical basis for the two models, then present each successively, and finally compare their predictions with the experimental results. Before proceeding, however, several qualitative remarks can already be made to inform the interpretation of the results presented above: (1) the fact that both resonances appear when the PNRs are known to form [2,4] (*breaking local inversion symmetry and locally inducing piezoelectricity*) at approximately 120 K for KLT3.5 and 140 K for KLT10, indicates that the PNRs must be the primary driver of these resonances, while the surrounding lattice remains cubic; (2) the observation of a pair of resonances rather than a single one in the frequency range for longitudinal oscillations of the bar samples suggests the existence of two distinct vibrational configurations or modes, corresponding respectively to in-phase and out-of-phase oscillations of the PNRs with the surrounding lattice or bar (see below); and (3) the asymmetric shape of the narrow resonance peak does seem to suggest the existence of a coupling between these two modes of oscillation. Next, we present each model successively and show that both describe the experimental spectra very well across the three temperature regions, quantitatively confirming the qualitative remarks made above.

A. Purely classical model

The observed resonance spectra can be explained phenomenologically in terms of the dynamics of the well-known classical system of two damped oscillators coupled to each other, as described by Eq. (1) [24,25]. In these equations, $X_{1,2}$ designates the displacements, $\gamma_{1,2}$ the damping coefficients and $\omega_{1,2}$ the radial frequencies of the two oscillators, ν_{12} the coupling coefficient between them, a_1 the drive amplitude of the first oscillator and ω the driving frequency. In the present KLT case, one of the oscillators is the PNRs and the other the surrounding lattice. The even normal mode of this coupled system corresponds to the PNRs and surrounding lattice oscillating in phase (both simultaneously in extension or contraction) and the odd mode, to them oscillating out-of-phase relative to each other:

$$\ddot{X}_1 + \gamma_1 \dot{X}_1 + \omega_1^2 X_1 - \nu_{12}^2 X_2 = a_1 \exp(-i\omega t),$$
$$\ddot{X}_2 + \gamma_2 \dot{X}_2 + \omega_2^2 X_2 - \nu_{12}^2 X_1 = 0. \quad (1)$$

These two normal modes can be coupled by flipping the displacement (deformation) vector of one of the two oscillators and correspondingly the relative phase of its motion by 180°. Because the surrounding lattice or macroscopic

bar sample is set into oscillations by the piezoelectric polar nanodomains, it should be clear that, initially, the ac field can only excite the even (primary) normal mode with displacement X_1. The latter can then couple to the odd (secondary) mode with displacement X_2 through the polarization and strain reversal of the PNRs, and vice versa (see schematic representation of the modes in the next section). At the higher temperature (region I), the two modes are coupled through the π relaxation or 180° polarization reversal of the piezoelectric PNRs, accompanied by a change of sign of their strain state from expansion to contraction. In the transition range (region III), they are coupled by the relaxation of the surrounding lattice between its higher temperature cubic and its lower temperature tetragonal phase (heterophase relaxation), also accompanied by a change of sign of the strain from expansion to contraction and vice versa.

The vibrational spectrum of such a well-known system does in fact reproduce very well the resonance spectra of KLT3.5 observed in both regions I and III. The experimental spectra and fits to the solution of Eq. (1) at 98 and 44 K are shown in Fig. 9 and the fitting parameters are listed in Table I. The quality of the fits to the experimental curves is excellent and the variation of the fitted values resulting from varying the starting values of the parameters is found to be less than 1%. As seen in Table I, the major differences between the two temperatures are (i) the much higher damping of the driven primary oscillator (broader resonance peak) but slightly lower damping of the secondary oscillator at 44 K than at 98 K and (ii) the smaller frequency separation and therefore greater overlap of the two resonances at 44 K $\approx$ 350 Hz than $\approx$800 Hz at 98 K. Despite the coupling coefficient ν_{12} being almost the same at the two temperatures, the fact that the two resonance peaks overlap significantly at the lower temperature translates into a higher transition probability between the two modes. As explained below, such a higher transition probability at 44 K can itself be explained by the proximity of the structural transition and the correspondingly much softer and deformable lattice.

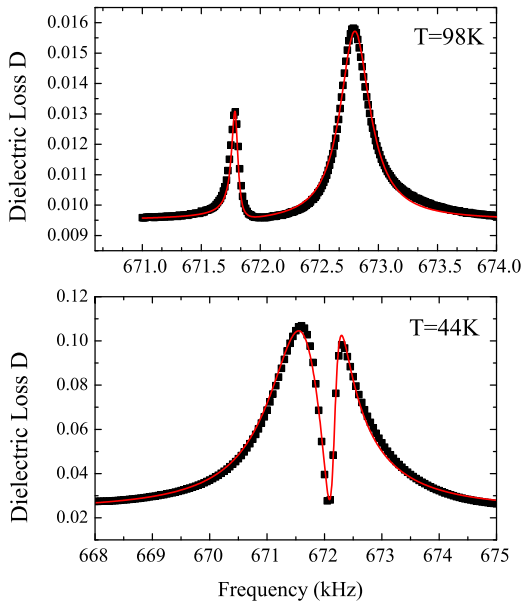

FIG. 9. Dielectric loss of KLT3.5 at 98 and 44 K (same data as in Fig. 3) fitted with the two coupled oscillators model described by Eq. (1).

TABLE I. Fit parameters from the purely classical model of two coupled damped harmonic oscillators.

Fit parameters	98 K	44 K
a_1	1.44×10^6	8.71×10^7
$\omega_1/2\pi$ (kHz)	672.69	671.75
$\omega_2/2\pi$ (kHz)	671.90	672.09
γ_1	340.9	1587.2
γ_2	32.1	17.8
ν_{12}	4.2×10^8	4.4×10^8
background	0.0095	0.0023

B. Semiclassical model

As an alternative to the purely classical model above, the observed spectrum of KLT3.5 can be described equally well by a semiclassical model, which contributes a complementary physical perspective on the results. As described by Fano, an asymmetric line shape such as that of the narrow peak results from the coherent mixing of a vibrational excitation from a ground state to a discrete excited state with a parallel excitation to a continuum, itself coupled to the same excited state [26]. The two coherently coupled parallel excitation paths lead to an interference. The Fano resonance picture can be extended to the case of two separate excitations between discrete energy levels which are coupled to each other through a continuum. In the context of KLT, the two separate excitations are the even and odd modes and the continuum corresponds to the relaxation coupling the two. Such a situation was modeled several years ago by Zawadowski and Ruvalds (ZR) [27] for the case of two discrete and long-wavelength optical phonons coupled to each other through pairs of acoustic phonons with wave vectors $+k$ and $-k$ and thus forming a continuum. The two-acoustic-phonon Green's function was taken to be purely imaginary, which is equivalent to a relaxation in the present KLT case. Given the one-to-one correspondence between the vibrational configuration described by ZR and the present one, we can directly use the spectral function given in Eq. (12) of their paper to describe the dielectric loss spectra in KLT:

$$\rho(\omega) = \frac{\epsilon''}{\epsilon'} = \frac{[Ag_a/2\Delta_a + Bg_b/2\Delta_b]^2}{1 + \left[g_a^2/2\Delta_a + g_b^2/2\Delta_b\right]^2} \qquad (2)$$

in which A and B are the oscillator strengths of the two normal modes, g_α their respective coupling coefficients to the relaxation and $\Delta_\alpha \equiv (1 - \frac{\omega}{\omega_\alpha})$ the relative frequency separation from their resonance frequencies. By contrast with the purely classical model described earlier by Eq. (1), in the semiclassical ZR model both discrete vibrational normal modes are assumed to be driven by the same external field instead of just the even (primary) mode. The fitted spectra of KLT3.5

are presented in Fig. 10 at 98 K, near the high-temperature anticrossing point in region I, and close to the transition in region III at 44 K. Here again, two seemingly very different spectra are fitted very well by the same model and we estimate the uncertainty on the fitted parameters to be less than 1%. The values of the fitting parameters are given in Table II. Unlike the fitting results obtained with the purely classical model, the respective frequencies of the two resonances are found here to be practically the same at 98 and 44 K.

In the present semiclassical model, the main difference between the spectra in regions I and III is the larger values of both coupling coefficients or widths of the resonances, g_a and g_b, which are twice as large at 44 K as they are at 98 K, while remaining in the same ratio, 1.3–1.4. This doubling results in the extensive overlap of the two resonances. This extensive overlap, and the resulting much larger transition probability between the two modes, appears to be the essential common feature of the two models. In the purely classical model, this overlap stems from a significant increase in the damping/width of the even (primary) mode and the reduced frequency separation between the two modes while, in the semiclassical model, it originates from an equal increase in the coupling coefficients of both modes to the acoustic continuum or relaxation. It is also important to note that the coupling between the two oscillators is taken into account differently in the two models. In the purely classical model, the primary (driven) mode is coupled to the secondary (slave) mode through an implicit continuum (the π or the heterophase relaxation), with the coupling expressed in the damping coefficient. In the semiclassical model by contrast, both oscillators are coupled explicitly to a common continuum, each with its own coupling coefficient.

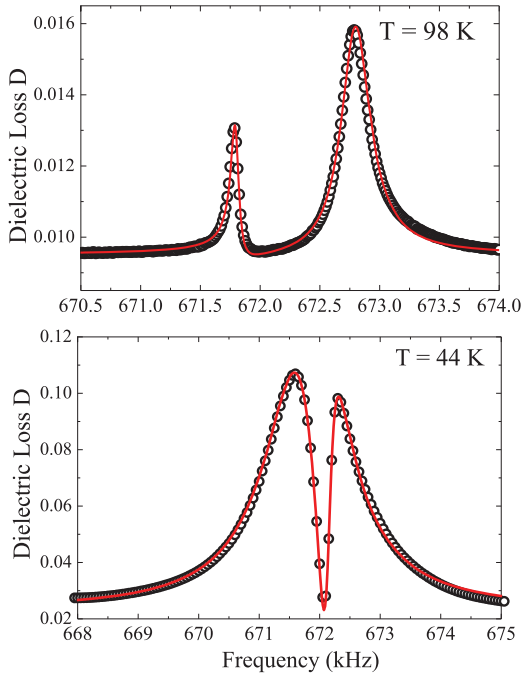

FIG. 10. Dielectric loss of KLT3.5 at 98 and 44 K (same data as in Fig. 3), fitted with the ZR model of Eq. (2).

TABLE II. Fit parameters from the semiclassical model of two discrete transitions coupled via a continuum.

Fit parameters	98 K	44 K
A	0.00169	0.0117
B	0.00106	0.0077
$\omega_a/2\pi$ (kHz)	672.51	671.57
$\omega_b/2\pi$ (kHz)	671.72	672.30
g_a	0.01855	0.04033
g_b	0.01451	0.028
background	0.0078	0.0231

IV. PHYSICAL DESCRIPTION AND DISCUSSION

In the present section, we describe a possible physical model that can explain the experimental results reported and analyzed in the two preceding section. Although there could be others, the validity of the proposed model rests on its ability to explain these results across the three temperature regions, I, II, and III. In each figure below, the PNRs are assumed to be aligned, at least partially, by the dc field while the ac field excites both resonances and relaxation. In region I, at high temperature, the even (in-phase) and odd (out-of-phase) normal modes of the PNRs-surrounding lattice system are coupled via the π relaxation of the lithium ions (red dots in Fig. 11), which switches the polarization of the PNRs (green arrows) by 180° and, correspondingly, their piezoelectric deformation from expansion or dilation to contraction. It should however be obvious that, initially, the ac field can only excite the coupled system in its even or in-phase mode since it is the piezoelectric deformation of the PNRs that initially drives the surrounding lattice and bar into oscillations. Only once the system has been set oscillating in the in-phase

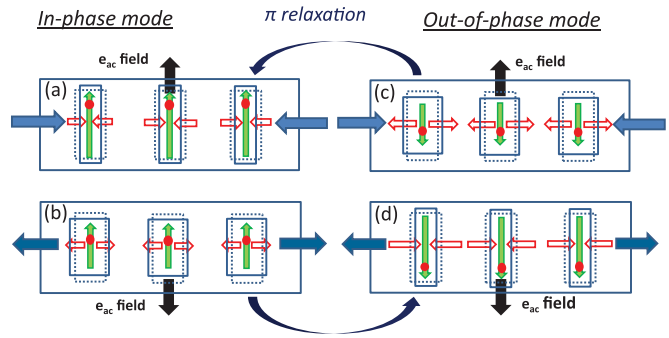

FIG. 11. Schematic representation of the modes of oscillations of the KLT crystal bar with PNRs partially aligned vertically in the dc electric field; the polarization of individual PNRs is represented by vertical green arrows and their deformation by horizontal open red arrows and dashed blue lines. The red dot inside each PND represents the lithium ions whose cooperative π relaxation is driven by the same ac electric field that drives the resonances. The position of the red dots can be seen to be related to the nature of the deformation of the PND (expansion or contraction). The deformation of the crystal bar is indicated by horizontal blue arrows. (a) and (b) correspond, respectively, to the polarized cubic (P_C) and strained cubic (S_C) states, and (c) and (d) to the polarized tetragonal (P_T) and strained tetragonal (S_T) states.

mode of vibration can it transition back and forth between the two modes through a reversal of the PND polarization and associated piezoelectric deformation triggered by the π relaxation.

One important aspect of the observed dynamics in region I is that it is coherent, since the same ac field that excites the piezoelectric resonance of the PNRs also triggers their π relaxation and accompanying 180° polarization reversal. Therefore, the π relaxation itself is not just thermally activated but assisted by the piezoelectric deformation of the PNRs, which reduces the potential barrier for the reorientation of the lithium ions and accompanying reversal of the PNRs polarization. And this process is clearly more effective for the in-phase or even mode since the deformations of the PNRs and surrounding lattice are then both of the same sign [see evolution from (b) to (c) or (d) in Fig. 11]. A stronger coupling to the relaxation means a higher damping of the in-phase mode and a broader resonance peak, as indeed observed.

Region II is the temperature region within which the $\pi/2$ relaxation reaches its maximum amplitude, $\omega\tau_{\pi/2} = 1$ (see Fig. 1). Unlike in region I, the 90° reorientation of the PNRs in region II does not couple the two oscillation modes to each other, and the out-of-phase mode (narrow asymmetric resonance) therefore vanishes (in KLT3.5) or is strongly suppressed (in KLT10). Additionally, and as seen in Figs. 3, 7, 5, and 8, the $\pi/2$ relaxation crosses over the frequency of the broad resonance, strongly damping it and depressing its frequency (as for a damped harmonic oscillator with increasing damping). The effect of the $\pi/2$ relaxation is illustrated in Fig. 12. This mechanism explains both the increased damping and associated rapid frequency decrease of the broad resonance and the total disappearance of the narrow resonance in KLT3.5 (and partial in KLT10), which only exists through its coupling to the broad resonance via the π relaxation. At lower temperatures, the $\pi/2$ relaxation itself slows down and in turn becomes inactive. As a result, the broad resonance is no longer damped, it recovers an even larger amplitude than before and its frequency increases again. The model used here to describe the evolution of the resonances in region II is therefore fully consistent with the model used in region I, itself based on the interaction of the resonance with a relaxation, π in regions I and $\pi/2$ in region II.

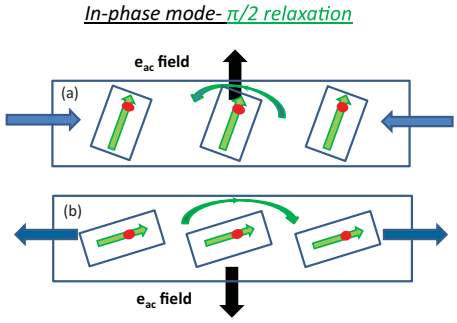

FIG. 12. The two half-cycles of PNRs undergoing a $\pi/2$ relaxation, which broadens the broad resonance and suppresses the narrow resonance; the features in this figure are the same as in the previous figure.

In region III, although the π and $\pi/2$ relaxations are no longer active, the two resonances nevertheless reappear, now strongly overlapping. The fact that the same two models are able to reproduce the experimental spectra in regions I and III indicates that a similar generic explanation must apply in both, in terms of two discrete oscillators (even and odd normal modes) coupled through a continuum (a relaxation). However, as already hinted above, the physical nature of the relaxation coupling the two modes is not the same in both regions. In region I, the even and odd modes correspond to the in-phase and out-of-phase oscillations of the PNRs-surrounding lattice system, coupled to each other through the π relaxation of the PNRs. However, region III lies well below the peak temperature of both relaxations, which are therefore inactive. The two modes must now be coupled through a different kind of relaxation, the nature of which is revealed by two observations: (i) region III straddles the structural transition, as shown by the hatched area in Fig. 1 and (ii) the thermal hysteresis seen in the inset of the same figure shows that region III is a region in which the high- and low-temperature phases are metastable on some time scale, but can relax from one to the other. These two observations suggest that the relaxation that is active in region III is the relaxation of the surrounding lattice between its high-temperature (cubic) and low-temperature (tetragonal) phases, otherwise called "heterophase fluctuations."

Heterophase fluctuations are indeed observed near weakly first-order transitions, where they are due to the presence of precursors of a low-temperature phase within a high-temperature equilibrium phase and vice versa [23,28,29]. Such fluctuations are quite naturally expected to occur in relaxors since the PNRs do indeed represent stable precursors of the low-temperature phase, already present above the transition. In the present case however, they are activated or assisted by the PNRs. Because the PNRs are intrinsically piezoelectric, modulation of their polarization by the ac field leads to a modulated stress on the surrounding lattice which, being already near a structural instability in the vicinity of the transition, can easily be made to transform (stress-induced) from the cubic to the tetragonal phase and vice versa. This stress-assisted transformation is necessarily accompanied by a phase change in the oscillations of the surrounding lattice relative to those of the PNRs, or coupling of the even/in-phase mode and the odd/out-of-phase mode as in region I. Here however, instead of the 180° PNR polarization relaxation being induced by the stress from the surrounding lattice or bar, it is now the surrounding lattice relaxation between the cubic and tetragonal phases that is induced by the piezoelectric deformation of the PNRs. Moreover, because the heterophase relaxation between the two phases is induced by the piezoelectric oscillations of the PNRs, it is also coherent with the latter. Figure 13 represents an attempt at illustrating the likely sequence for the resonance-relaxation process in which the ac field again modulates the polarization of the PNRs whose deformation drives the heterophase relaxation of the surrounding lattice and ultimately the macroscopic bar oscillations. Here, in region III, we should note that the sequence of the oscillations is (a)-(d)-(c)-(b)-(a) because the switch from the even to the odd mode is due to the cubic-tetragonal transformation of the surrounding lattice whereas, in region I, it was due to the reversal of polarization and

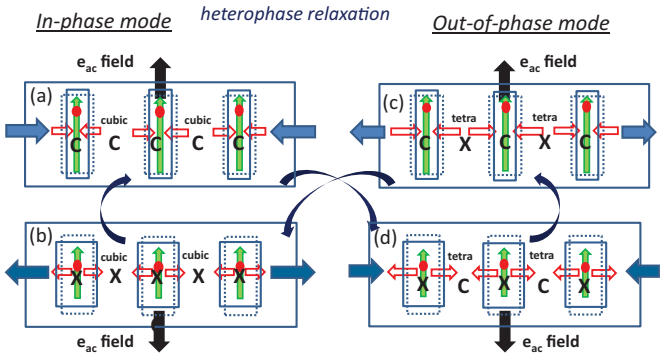

FIG. 13. Normal modes of oscillations of the PNRs and surrounding lattice in the transition region. The color codes are the same as in the region I representation. At the lower temperature of the transition however, both the π and $\pi/2$ relaxations are inactive and the PNR polarization remains aligned along the dc field, upward in the picture. C and X designate contraction and expansion, respectively, and the crystal symmetry of the surrounding lattice is also indicated. Following the ac field, the system evolves along the path (a)-(d)-(c)-(b)-(a) or, according to the labels of Fig. 11 from P_C to S_T, P_T, S_C, and back to P_C. Starting from the in-phase mode half-cycle (a), the surrounding lattice between PNRs is cubic but its contraction under the opposite deformations of the PNRs and the bar induces a transition to the tetragonal phase in (d). Similarly, its expansion in (c) induces a transition back to the cubic phase in (b).

accompanying piezoelectric strain of the PNRs. Hence the two coupled-mode picture that explains the dynamics in region I is also valid in region III, although the physical nature of the relaxation coupling the two modes is different in the two regions.

Starting with half-cycle (a) and the cubic lattice, the combination of the dc and ac fields enhances the polarization of the PNRs which contract (C), resulting in the contraction of the surrounding lattice and bar sample. The latter contraction then induces the cubic-to-tetragonal transformation of the lattice in half-cycle (d), which maintains the bar in contraction while the ac field has reversed and the PNRs are now expanding. The PNRs-surrounding lattice system now oscillates in the odd mode. In half-cycle (c), with the reversal of the ac field but still in the out-of-phase mode, the PNRs now contract while the surrounding lattice expands, inducing the reverse tetragonal-to-cubic transformation of the lattice and coupling the odd mode back to the even mode in half-cycle (b). Here we note that the two half-cycles (a) and (b) of the even mode in the cubic lattice are identical to those in Fig. 11, but that the two half-cycles (c) and (d) of the odd mode are inverted compared to the previous ones due to the cubic-tetragonal heterophase relaxation. The proposed model is again consistent with the lower frequency and much higher damping coefficient of the even (in-phase) mode.

We now address the question of the coherence between the in-phase and out-of-phase oscillations (even and odd modes) of the system, a coherence that is essential to the efficient transfer of energy between them. This coherence is evidenced by the Fano-like asymmetry of the narrow resonance peak at higher temperature in region I and in the transition region III by the sharp wedge between the two resonances in Fig. 3 at 48 and 44 K or in Fig. 5 at 72 and 68 K (see circled anti-resonances, as in Refs. [26,27]). These characteristic line shapes are signatures of coherent effects and indicate that the relaxation coupling the in-phase and out-of-phase oscillations is not simply thermally activated but assisted by these oscillations, both being excited coherently by the same ac electric field. In region I, the two modes are coupled to each other via the 180° or π relaxation of the PNRs, which is facilitated/assisted by the deformation of the surrounding lattice and bar. In region III, where the π relaxation is no longer active, the relaxation that couples the two oscillation modes is now the structural transformation of the surrounding lattice from cubic to tetragonal, which is stress-induced by the piezoelectric PNRs. This explains the 4.6 fold increase in the damping of the driven primary oscillator in the purely classical model and the doubling of both coupling coefficients in the semiclassical model. Both are therefore coherent effects.

The necessary condition for the observation of coupled resonances such as those reported above in KLT is the presence of piezoelectric polar nanodomains with orientational degrees of freedom. These are in fact the characteristic features of relaxor ferroelectrics. It is therefore not surprising that similar resonances have also been observed in other relaxors, $KTa_{1-x}Nb_xO_3$ (KTN), $PbMg_{1/3}Nb_{2/3}O_3$ (PMN) [12], and $PbZn_{1/2}Nb_{1/2}O_3$ (PZN). The present report on the PNR-related resonances observed in KLT, and their analysis and interpretation, should therefore contribute broadly to a better understanding of the multiscale dynamics in relaxor ferroelectrics, explaining how their macroscopic properties emerge from their structural and dynamical properties at the nanolevel.

Besides their contribution to a better understanding of relaxor ferroelectrics, the above results may also be of a general interest in condensed matter physics. Relaxor ferroelectrics are but one example of what can be called coherent nanocomposites. Such systems are characterized by a nanometer scale local order that is structurally coherent with the surrounding lattice, as in relaxor ferroelectrics. Similar types of phenomena as those described in the present paper are likely to be observed for instance in nanocomposite magnetic systems [30]. The resonance phenomena reported here may also be of interest at a more general physical level. They are indeed conceptually similar to phenomena observed in very different fields of physics, and in particular electromagnetically induced transparency (EIT) in atomic physics. The dielectric susceptibility spectra reported above in the relaxor KLT near the phase transition are indeed almost identical to the optical susceptibility spectra resulting from EIT in atomic vapors and reproduced here in Fig. 14 for rubidium from Ref. [31] (compare with the KLT spectra in Figs. 3 and 5).

The physical model used to describe the resonance phenomenon in KLT can in fact also be described semiclassically by analogy with the formalism of EIT for an atom with three discrete states [a ground state (1) and two coupled excited states (2,3)] exhibiting two closely spaced lifetime-broadened resonances that decay to the same continuum [32] (see also [33]). In KLT, the ground state corresponds to the polarized state and the two excited states to the in-phase and out-of-phase strained states of the PNR-surrounding lattice system. The energy width of the two excited states is associated with

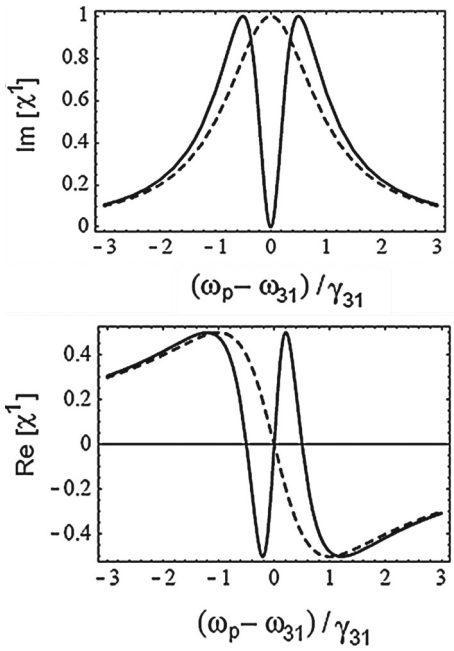

FIG. 14. Imaginary (top) and real (bottom) parts of the optical susceptibility of an atomic rubidium vapor [31]. ω_p is the probe (laser) frequency, ω_{31} and γ_{31} the resonant frequency and damping, respectively, of the primary transition [in KLT, (1) would be the polarized state and (3) the in-phase strained state of the PNRs-surrounding lattice system with state (2) corresponding to the out-of-phase strained state]. The dash curve corresponds to the susceptibility of a usual two state system (1-3), which does not exhibit EIT.

the damping of the oscillators in the classical model and with the coupling strength of the two oscillators to the continuum in the semiclassical model, both contributing to the overlap between the states and increased coherency between the two resonances. The correspondence of the coherent dynamics of KLT and other relaxors with EIT will be further explored in a subsequent paper.

In conclusion, we have reported the observation and provided a comprehensive explanation of pairs of coupled resonances in the relaxor ferroelectric $K_{1-x}Li_xTaO_3$ (KLT). Similar resonances are also observed in other relaxors such as $KTa_{1-x}Nb_xO_3$ (KTN) but also PMN and PZN. These resonances provide a window into the multiscale dynamics of complex oxides, from the nanometer to the macrometer scale. They are shown to be associated with two distinct oscillating configurations or normal modes of the nanocomposite PNRs-surrounding lattice system, coherently coupled to each other via a relaxation. The observed spectra exhibit characteristic Fano lineshapes that evolve rapidly through three temperature ranges due to the complex interactions between resonances and relaxations. Despite this rapid evolution, the resonance spectra are explained and fitted equally well over the entire temperature range using either one of two models, a purely classical or a semiclassical model, each highlighting a particular aspect of the dynamics of the system. Similar spectra are observed in other relaxors, pointing to the generality of these results. It may also be worth mentioning that other types of measurements have also revealed Fano line shapes in disordered relaxor ferroelectrics, even though these have been observed in the THz frequency range and may therefore have different physical origins [34,35]. Finally, and of possibly broader significance, the spectral line shapes reported and analyzed in the present study are shown to be identical to those observed in the optical spectra of atomic vapors as a result of electromagnetically-induced transparency (EIT) and the conceptual similarity between the two phenomena is noted.

ACKNOWLEDGMENTS

The early part of this work was supported by a grant from the US Department of Energy, Office of Basic Energy Sciences, DE-FG02-06ER46318 and the NSF-REU program (JL). We also wish to thank Dr. L.A. Boatner from the Oak Ridge National Laboratory for providing the crystals used in the present study. Special thanks to J.F. Scott for pointing out the ZR paper to us.

[1] I.-K. Jeong, T. W. Darling, J. K. Lee, T. Proffen, R. H. Heffner, J. S. Park, K. S. Hong, W. Dmowski, and T. Egami, Phys. Rev. Lett. **94**, 147602 (2005).
[2] J. Toulouse, P. DiAntonio, B. E. Vugmeister, X. M. Wang, and L. A. Knauss, Phys. Rev. Lett. **68**, 232 (1992).
[3] G. Xu, Z. Zhong, H. Hiraka, and G. Shirane, Phys. Rev. B **70**, 174109 (2004).
[4] G. Yong, J. Toulouse, R. Erwin, S. M. Shapiro, and B. Hennion, Phys. Rev. B **62**, 14736 (2000).
[5] The label polar nanoregions (PNRs) does not distinguish between temperature ranges in which the local order is temporary or dynamic and those ranges in which it becomes permanent, implying a lowering of the local symmetry, local polarization and piezoelectric character. Earlier authors have also made that distinction, e.g., Samara in Phys. Rev. Lett. **77**, 314 (1996).
[6] A. A. Bokov and Z.-G. Ye, J. Mater. Sci. **41**, 31 (2006).
[7] J. Toulouse, B. E. Vugmeister, and R. K. Pattnaik, Phys. Rev. Lett. **73**, 3467 (1994).
[8] C.-S. Tu, F.-T. Wang, R. R. Chien, V. H. Schmidt, and L.-C. Lim, J. Appl. Phys. **100**, 074105 (2006).
[9] N. D. Sharma, R. Maranganti, and P. Sharma, J. Mech. Phys. Solids **55**, 2328 (2007).
[10] N. Cereceda, B. Noheda, J. R. Fdez.-del-Castillo, J. A. Gonzalo, J. De Frutos, and A. M. Gonzalez, J. Eur. Ceram. Soc. **19**, 1259 (1999).
[11] S. E. Park and T. R. Shrout, J. Appl. Phys. **82**, 1804 (1997).
[12] R. K. Pattnaik and J. Toulouse, Phys. Rev. Lett. **79**, 4677 (1997).
[13] R. K. Pattnaik and J. Toulouse, Phys. Rev. B **60**, 7091 (1999).
[14] V. I. Yukalov, Phys. Rep. **208**, 395 (1991).
[15] Y. Yacoby, W. B. Holzapfel, and D. Bauerle, Solid State Commun. **23**, 947 (1977).
[16] R. K. Pattnaik, J. Toulouse, and B. George, Phys. Rev. B **62**, 12820 (2000).
[17] L. A. Knauss, X. M. Wang, and J. Toulouse, Phys. Rev. B **52**, 13261 (1995).

[18] P. Doussineau, Y. Farssi, C. Fresnois, A. Levelut, J. Toulouse, and S. Ziolkiewicz, Ferroelectrics **150**, 59 (1993).
[19] J. J. van der Klink, D. Rytz, F. Borsa, and U. T. Hochli, Phys. Rev. B **27**, 89 (1983).
[20] J. Toulouse and B. Hennion, Phys. Rev. B **49**, 1503 (1994).
[21] G. A. Azzini, G. P. Banfi, E. Giulotto, and U. T. Hochli, Phys. Rev. B **43**, 7473 (1991).
[22] P. Doussineau, Y. Fresnois, A. Levelut, K. McEnaney, J. Toulouse, and S. Ziolkiewic, Europhys. Lett. **24**, 415 (1993).
[23] A. Gordon, J. Phys. C **20**, L111 (1987).
[24] Y. S. Joe, A. M. Satanin, and S. C. Kim, Phys. Scr. **74**, 259 (2006).
[25] C. L. Garrido Alzar, M. A. G. Martinez, and P. Nussenzveig, Am. J. Phys. **70**, 37 (2002).
[26] U. Fano, Phys. Rev. **124**, 1866 (1961).
[27] A. Zawadowski and J. Ruvalds, Phys. Rev. Lett. **24**, 1111 (1970).
[28] J. Brookeman and A. Rigamonti, Phys. Rev. B **24**, 4925 (1981).
[29] H. E. Cook, Phys. Rev. B **15**, 1477 (1977).
[30] T. Kimura, Y. Tomioka, R. Kumai, Y. Okimoto, and Y. Tokura, Phys. Rev. Lett. **83**, 3940 (1999).
[31] M. Fleischhauer, A. Imamoglu, and J. P. Marangos, Rev. Mod. Phys. **77**, 633 (2005).
[32] S. E. Harris, J. E. Field, and A. Imamoglu, Phys. Rev. Lett. **64**, 1107 (1990).
[33] J. P. Marangos, J. Mod. Opt. **45**, 471 (1998).
[34] M. M. Rahaman, T. Imai, T. Sakamoto, S. Tsukada, and S. Kojima, Sci. Rep. **6**, 23898 (2016).
[35] D. Wang, J. Hlinka, A. A. Bokov, Z.-G. Ye, P. Ondrejkovic, J. Petzelt, and L. Bellaiche, Nat. Commun. **5**, 5100 (2014).